Mon. Not. R. Astron. Soc. **373,** 836–844 (2006) doi:10.1111/j.1365-2966.2006.11088.x

Pulse profiles of millisecond pulsars and their Fourier amplitudes

Juri Poutanen[1]★ and Andrei M. Beloborodov[2,3]★

[1]*Astronomy Division, PO Box 3000, FIN-90014 University of Oulu, Finland*
[2]*Physics Department and Columbia Astrophysics Laboratory, Columbia University, 538 West 120th Street, New York, NY 10027, USA*
[3]*Astro Space Center, Lebedev Physical Institute, Profsojuznaja 84/32, 117810 Moscow, Russia*

Accepted 2006 September 20. Received 2006 August 30

ABSTRACT

Approximate analytical formulae are derived for the pulse profile produced by small hotspots on a rapidly rotating neutron star. Its Fourier amplitudes and phases are calculated. The proposed formalism takes into account gravitational bending of light, Doppler effect, anisotropy of emission and time delays. Its accuracy is checked with exact numerical calculations.

Key words: stars: neutron – pulsars: general – X-rays: binaries.

1 INTRODUCTION

During the past decade, coherent (or nearly coherent) oscillations in the ∼200–600 Hz frequency range were discovered in the light curves of a number of neutron stars in low-mass X-ray binaries observed by the *Rossi X-ray Timing Explorer* (*RXTE*). In 13 sources, these oscillations were discovered during X-ray bursts (see Strohmayer & Bildsten 2006, for a review), giving the name *nuclear-powered millisecond pulsars* to this class of objects. Seven transient sources, *accretion-powered millisecond pulsars*, showed coherent pulsations in the persistent flux during the outbursts lasting a few weeks (see reviews by Poutanen 2006; Wijnands 2006). In all these millisecond pulsars (hereafter MSP), the observed emission is dominated by bright spots on the neutron star surface. Such bright spots are created either by a thermonuclear explosion observed as an X-ray burst or by an accretion flow channelled towards a magnetic pole. The pulse profile produced by the spot carries information about the position of the spot, its size, spectrum and angular distribution of its emission and the gravitational field of the star.

The X-ray pulse profiles observed from MSP are almost sinusoidal. In SAX J1808.4−3658 (Gierliński, Done & Barret 2002; Poutanen & Gierliński 2003) and XTE J1814−338 (Strohmayer et al. 2003), there is a notable skewing of the profile which increases with photon energy. The skewness as well as the observed soft time lags probably result from Doppler boost of anisotropically emitted radiation (Gierliński et al. 2002; Poutanen & Gierliński 2003). Pulse profiles of SAX J1808.4−3658 have been measured with high accuracy at different photon energies and well fitted by a theoretical model (Poutanen & Gierliński 2003). This gave constraints on the neutron star radius $8 < R < 12$ km (assuming mass of 1.4–1.6 $M_\odot$) and on the inclination of the spin axis to the line of sight $i \gtrsim 60^\circ$.

The poor photon statistics available for MSP normally does not allow one to study in detail the shapes of their light curves. Therefore, data analysis is often limited to the amplitude and phase of the fundamental Fourier harmonic, and sometimes higher harmonics may be analysed. The Fourier technique helps to use the available data to constrain the neutron star parameters (see e.g. Miller & Lamb 1998; Weinberg, Miller & Lamb 2001; Muno et al. 2002; Gierliński & Poutanen 2005). A number of recent papers were devoted to numerical calculations of the amplitude of pulsations created by a spot (or two antipodal spots) for different radiation patterns, rotational velocities, inclinations, spot positions and their sizes (see e.g. Weinberg et al. 2001; Muno et al. 2002). Such calculations involve light-bending and Doppler effects, which made the problem complicated and required numerical calculations. Given the large number of parameters, the numerical approach makes it difficult to understand the dependence of results on parameters and interpret the data.

The purpose of this paper is to develop an approximate analytical description of the problem. Using the simple formalism of Beloborodov (2002, hereafter B02) for light bending, we derive analytical formulae for oscillation amplitudes which demonstrate how the observables depend on the parameters of the problem.

The plan of this paper is as follows. In Section 2, we introduce our notations and summarize the exact numerical method of the light-curve calculation. In Section 3 we discuss the approximate description of light bending, introduce an approximate formula for time-delay effects, describe possible classes of MSP and finally derive approximate analytical formulae for the pulse profiles and the corresponding amplitudes and phases of the Fourier series. Using our analytical formalism, we compare the approximate Fourier amplitudes to the exact results and investigate the effects of anisotropy of the emission pattern and the Doppler effect on the pulse profile in Section 4.

2 PULSE FROM A SPOT ON A SPINNING STAR

Consider a small spot on the star surface. Its area measured in the corotating frame is $\mathrm{d}S'$, and its instantaneous position in the fixed lab frame is described by the unit vector $\boldsymbol{n}$ that points to the spot from the star centre (see Fig. 1). The angle between $\boldsymbol{n}$ and the line of sight is denoted by ψ. We are interested in photons emitted by the

★E-mail: juri.poutanen@oulu.fi (JP); amb@phys.columbia.edu (AMB)

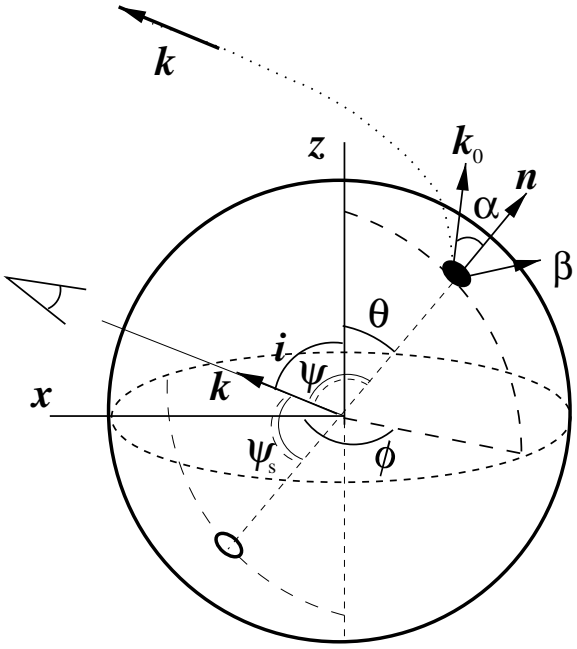

Figure 1. Geometry of the problem. Dotted curve shows the photon trajectory.

spot that propagate along our line of sight at large distances from the star (where gravitational bending becomes negligible). We denote the unit vector along the line of sight by $\boldsymbol{k}$, so that

$$\cos\psi = \boldsymbol{k}\cdot\boldsymbol{n}. \tag{1}$$

As the star rotates, $\boldsymbol{k}\cdot\boldsymbol{n}$ varies periodically,

$$\cos\psi = \cos i\ \cos\theta + \sin i\ \sin\theta\ \cos\phi, \tag{2}$$

where i is the inclination angle of the spin axis to the line of sight, θ is the spot colatitude and $\phi = 2\pi\nu t$ is the rotational phase of the pulsar; $\nu = P^{-1}$ is the pulsar frequency and $t = 0$ is chosen when the spot is closest to the observer.

Angle ψ measures the apparent inclination of the spot to the line of sight, which is different from the true inclination because of the light-bending effect. We denote the initial direction of the emitted photon by $\boldsymbol{k}_0$ and the true emission angle by α, so that

$$\cos\alpha = \boldsymbol{k}_0\cdot\boldsymbol{n}. \tag{3}$$

Emission angle in the corotating frame is denoted by α'. It differs from α because of relativistic aberration (see derivation in Appendix A):

$$\cos\alpha' = \delta\ \cos\alpha, \tag{4}$$

where $\delta = 1/\gamma(1-\beta\cos\xi)$ is the Doppler factor. Here $\gamma = (1-\beta^2)^{-1/2}$ and $\beta = v/c$ is the spot velocity,

$$\beta = \frac{2\pi R}{c}\frac{\nu}{\sqrt{1-u}}\sin\theta = \beta_{\rm eq}\sin\theta, \tag{5}$$

$\beta_{\rm eq}$ is the velocity at the equator and ξ is the angle between the spot velocity and $\boldsymbol{k}_0$. Here $u \equiv r_{\rm S}/R, r_{\rm S} = 2GM/c^2$ is the Schwarzschild radius; M and R are the mass and radius of the star. The pulsar frequency has been corrected for the redshift $\sqrt{1-u}$. One can show that ξ is related to α, ψ, i and ϕ by (see Appendix A),

$$\cos\xi = -\frac{\sin\alpha}{\sin\psi}\sin i\ \sin\phi. \tag{6}$$

For power-law spectra (observed for example in accretion-powered MSP), we assume that the energy and angular dependencies of the spectrum emitted by the spot may be separated as

$$I_{E'}(\alpha') = I_0(1 + h\cos\alpha')E'^{-(\Gamma-1)}, \tag{7}$$

where h does not depend on the photon energy E. If the power-law spectrum is produced by the thermal Comptonization by electrons of temperature $T_{\rm e}$, this condition would be satisfied if the maximum Doppler shift $\Delta\delta \sim 2\pi\nu R/c\sin i\sin\theta$ is smaller than the typical relative energy change in a single scattering $\Delta E/E \sim 4kT_{\rm e}/m_{\rm e}c^2$, which translates to $(\nu/600\,{\rm Hz})\sin i\sin\theta < kT_{\rm e}/16\,{\rm keV}$ (Viironen & Poutanen 2004). Even for X-ray burst spectra one expects that h varies slowly with energy, so that equation (7) still can be used.

The observed spectral flux at a distance D from the star is then given by (see derivation in Appendix A),

$$F_E = (1-u)^{\Gamma/2}\ \delta^{\Gamma+3} I'_E(\alpha')\cos\alpha\ \frac{{\rm d}\cos\alpha}{{\rm d}\cos\psi}\ \frac{{\rm d}S'}{D^2}. \tag{8}$$

Expression for the bolometric flux may be obtained as a special case of equation (8) by setting $\Gamma = 2$,

$$F = (1-u)\ \delta^5\ I'(\alpha')\ \cos\alpha\ \frac{{\rm d}\cos\alpha}{{\rm d}\cos\psi}\ \frac{{\rm d}S'}{D^2}. \tag{9}$$

These equations take into account the special relativistic effects (Doppler boost, relativistic aberration) as well as general relativistic effects (gravitational redshift and light bending in Schwarzschild geometry).

For further analysis, we use pulse profiles normalized to $F_0 = I_0\,E^{-(\Gamma-1)}\,(1-u)^{(\Gamma+2)/2}\,{\rm d}\,S'/D^2$:

$$F(\phi) = \delta^{\Gamma+3}(1 + h\delta\cos\alpha)\cos\alpha\ \frac{1}{1-u}\ \frac{{\rm d}\cos\alpha}{{\rm d}\cos\psi}. \tag{10}$$

The flux is zero if $\cos\alpha < 0$. For the antipodal spot, we substitute $\theta \to \pi - \theta$ and $\phi \to \pi + \phi$.

Expression (10) does not account for time delays resulting from different paths travelled by photons emitted at different phases ϕ. The delays become significant only for very fast-rotating pulsars. In Schwarzschild metric, the maximum time delay for a neutron star of $M = 1.4\,{\rm M}_\odot$ is $\Delta t \sim 7\times10^{-2}$ ms (almost independent of compactness of the star M/R). This gives at most a 5 per cent correction to the arrival phase for a rotational period $P = 1.5$ ms. The flux at observed phase $\phi_{\rm obs}$ is $\bar{F}(\phi_{\rm obs}) = F(\phi_{\rm obs} - \Delta\phi)$ with phase delay $\Delta\phi = 2\pi\nu\Delta t$ computed using (A17) and (A18) from the appendix. The effect of the photon arrival time contraction (or stretching) on the observed flux is already accounted for by one of the Doppler factors. The effects of gravitational bending, Doppler boost and time delays on the pulse profile are shown in Fig. 2.

Fourier series of the pulse profile is given by

$$\bar{F}(\phi_{\rm obs}) = A_0 + \sum_{n=1}[A_n\cos(n\phi_{\rm obs}) + B_n\sin(n\phi_{\rm obs})], \tag{11}$$

where

$$\begin{aligned} A_0 &= \frac{1}{2\pi}\int_0^{2\pi}\bar{F}(\phi_{\rm obs})\,{\rm d}\phi_{\rm obs},\\ A_n &= \frac{1}{\pi}\int_0^{2\pi}\bar{F}(\phi_{\rm obs})\cos(n\phi_{\rm obs})\,{\rm d}\phi_{\rm obs},\ n \geqslant 1\\ B_n &= \frac{1}{\pi}\int_0^{2\pi}\bar{F}(\phi_{\rm obs})\sin(n\phi_{\rm obs})\,{\rm d}\phi_{\rm obs},\ n \geqslant 1. \end{aligned} \tag{12}$$

An alternative form of Fourier series is written in terms of amplitudes c_n and phases $\Delta\phi_n$

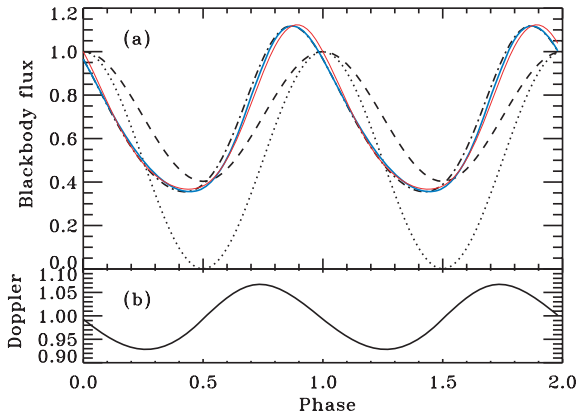

Figure 2. (a) The bolometric blackbody flux as a function of the observed phase. Dotted curve is for a slowly rotating star ignoring all relativistic effects. The pulse profile where gravitational light bending is accounted for is shown by the dashed curve. Dot–dashed curve gives the profile modified by the Doppler boost and aberration for a neutron star rotational frequency $\nu = 600$ Hz. Solid curve accounts also for the time delay. Thin solid curve is a pulse profile produced using the approximate Fourier amplitudes derived in Section 3. (b) Doppler factor δ as a function of the observed phase for $\nu = 600$ Hz. We take $i = \theta = 45^\circ$, $R = 2.5r_S$ and $M = 1.4\,M_\odot$ in this example.

$$\bar{F}(\phi_{\rm obs}) = \sum_{n=0} C_n \cos[n(\phi_{\rm obs} + \Delta\phi_n)], \tag{13}$$

where

$$C_n = \sqrt{A_n^2 + B_n^2}, \quad \tan(n\Delta\phi_n) = \frac{-B_n}{A_n}. \tag{14}$$

The exact Fourier series are calculated numerically.

3 ANALYTICAL APPROXIMATION

3.1 Light bending and time delay

The expressions for the observed flux (8) and (9) can be significantly simplified if one uses analytical formula for light bending and time delays. This will allow us to also obtain analytical expressions for the pulsation amplitude and Fourier harmonics in Section 3.3.

Beloborodov (2002) showed that the relation

$$\cos\alpha \approx u + (1-u)\cos\psi \tag{15}$$

describes light bending with high accuracy (see also Leahy & Li 1995; Zavlin, Shibanov & Pavlov 1995, for discussion of approximations). The accuracy of equation (15) is shown in Fig. 3 (see also B02). For a star with $R = 2r_S$, the accuracy is better than 10 per cent, while for $R = 3r_S$ the error does not exceed 3 per cent. The spot is visible to the observer when

$$\cos\psi > \cos\psi_{\rm max} = \frac{-u}{1-u}. \tag{16}$$

The exact expression for the time delays (A17) may also be approximated by a simple formula. Expanding it in Taylor series with $1 - \cos\alpha$ as a small parameter and using also the expansion

$$\frac{1-\cos\alpha}{1-u} = y\left(1 + \frac{u^2}{112}y^2\right) \tag{17}$$

(obtained from equation 2 in B02), where $y = 1 - \cos\psi$, we get

$$\Delta t = y\left\{1 + \frac{uy}{8}\left[1 + y\left(\frac{1}{3} - \frac{u}{14}\right)\right]\right\}\frac{R}{c}. \tag{18}$$

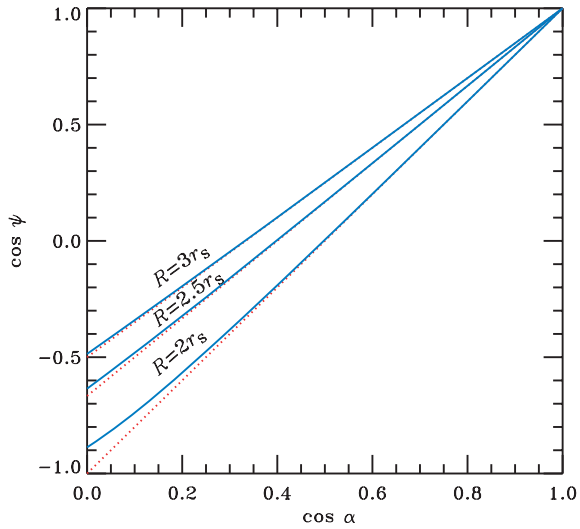

Figure 3. Light bending in Schwarzschild metric. The solid curves are the exact results using equation (A1) and the dotted lines is the approximation (15).

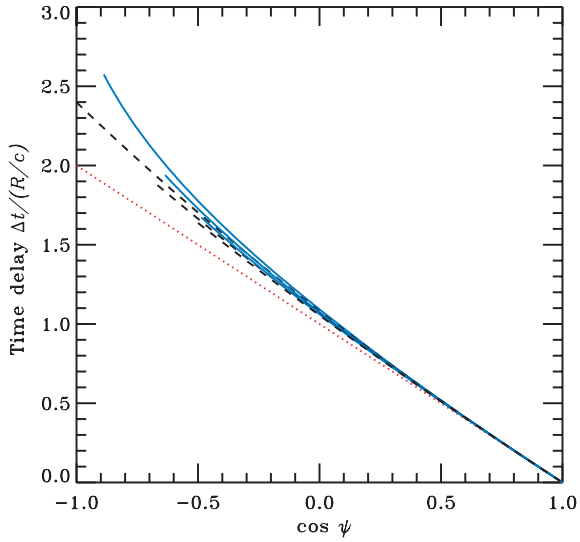

Figure 4. Time delays in Schwarzschild metric. The solid curves are the exact results using equation (A17) for $R = 2$, 2.5 and $3r_S$ (from top to bottom). The dashed curves show the results of an approximate formula (18), and the dotted line is the approximation (19).

Keeping only the leading term, we find

$$\Delta t = y\frac{R}{c}. \tag{19}$$

This approximation is better than 20 per cent accurate for most emission angles and compactnesses (Fig. 4). Only in the extreme case of $R = 2r_S$ for large bending angles (and large delays), the error increases to 35 per cent. Since the time delays themselves produce a small effect, equation (19) is sufficient in most calculations.

3.2 Pulsar visibility classes

Analytical light-bending formula (15) allows one to introduce a simple classification of the light curves according to the relative positions of $\mu_{\rm min} \equiv \cos(i+\theta)$, $\mu_{\rm max} \equiv \cos(i-\theta)$, $\cos\psi_{\rm max}$ and

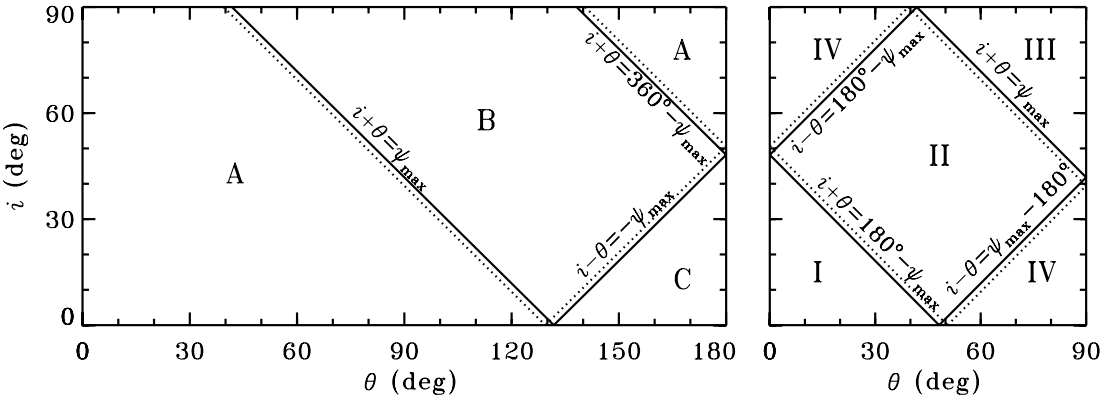

Figure 5. Classes of visibility for hotspots on neutron star surface at the inclination i – spot colatitude θ plane. The classes are determined by the relative positions of $\mu_{\min} = \cos(i+\theta), \mu_{\max} = \cos(i-\theta), \cos\psi_{\max}$ and $\kappa \equiv |\cos\psi_{\max}|$. Left-hand panel: classes for one spot. In class A defined by $\mu_{\min} > -\kappa$, the spot is always visible. In class B defined by $\mu_{\min} < -\kappa < \mu_{\max}$, the spot is not visible for a fraction of period. In class C defined by $\mu_{\max} < -\kappa$, the spot is never visible. Right-hand panel: classification for two antipodal spots as given in B02. In class I, $\mu_{\min} > \kappa$, the primary spot is visible all the time and the antipodal spot is never seen. In class II, $-\kappa < \mu_{\min} < \kappa < \mu_{\max}$, the primary spot is seen all the time and the antipodal spot also appears for some time. In class III, $\mu_{\min} < -\kappa$, the primary spot is not visible for a fraction of period (and then only the antipodal spot is seen). In class IV, $-\kappa < \mu_{\min}, \mu_{\max} < \kappa$, both spots are seen at any time. Dotted and solid lines correspond to the exact $\psi_{\max} = 129.^{\circ}4$ and approximate $\cos\psi_{\max} = -u/(1-u)$ (giving $\psi_{\max} = 131.^{\circ}8$), for $u = 0.4$ (i.e. $R = 2.5r_{\rm S}$).

$\kappa \equiv |\cos\psi_{\max}|$. For a single spot, three classes exist (see the left-hand panel of Fig. 5). In class A, defined by $\mu_{\min} > -\kappa$, the spot is always visible. When $\kappa < -\mu_{\max}$ (class C), the spot is always invisible. For $\mu_{\min} < -\kappa < \mu_{\max}$ (class B), the spot is visible during the pulsar phases $|\phi| < \phi_{\rm p}$, where

$$\cos\phi_{\rm p} = \frac{\cos\psi_{\max} - \cos i\cos\theta}{\sin i\sin\theta} = \frac{-Q}{U}, \tag{20}$$

and we defined

$$U = (1-u)\sin i\ \sin\theta,$$
$$Q = u + (1-u)\cos i\ \cos\theta. \tag{21}$$

Pulsars with two antipodal spots are divided into four classes (shown in the right-hand panel of Fig. 5, see also B02). In class I, corresponding to $\mu_{\min} > \kappa$ only the primary spot is visible all the time. In class II, $-\kappa < \mu_{\min} < \kappa < \mu_{\max}$, the primary spot is always visible, while the antipodal secondary spot appears during phases $\phi_{\rm s} < \phi < 2\pi - \phi_{\rm s}$, where

$$\cos\phi_{\rm s} = -\frac{\cos\psi_{\max} + \cos i\cos\theta}{\sin i\sin\theta} = \frac{2u-Q}{U}. \tag{22}$$

The primary spot disappears for a fraction of the period in class III, $\mu_{\min} < -\kappa$, and then only the antipodal spot is seen. And finally, in class IV ($-\kappa < \mu_{\min}, \mu_{\max} < \kappa$), both spots are seen all the time.

3.3 Fourier series

Our aim is to obtain simple analytical expressions for the Fourier amplitudes and phases characterizing the pulse profile. We can simplify expression (10) by using approximation to the light-bending formula (15):

$$F(\phi) = \delta^{\Gamma+3}(1 + h\delta\cos\alpha)\cos\alpha, \tag{23}$$

where now

$$\cos\alpha = Q + U\cos\phi. \tag{24}$$

Doppler factor δ depends on $\beta_{\rm eq}$. In the leading order of $\beta_{\rm eq} \ll 1$, this dependence is given by

$$\delta \approx 1 - \beta_{\rm eq}\sin i\ \sin\theta\frac{\sin\alpha}{\sin\psi}\sin\phi. \tag{25}$$

We further approximate $\sin\alpha/\sin\psi \approx \sqrt{1-u}$ which becomes exact at $\alpha \ll 1$ (cf. the cosine relation 15). This gives

$$\delta \approx 1 - T\sin\phi, \tag{26}$$

where

$$T \equiv \beta_{\rm eq}\sqrt{1-u}\ \sin i\ \sin\theta \ll 1. \tag{27}$$

Hereafter, we keep linear terms in T and neglect higher order terms. Then, substituting δ into expression (23), we obtain the flux (as a function of ϕ):

$$F(\phi) = a_0 + \sum_{n=1}^{3}[a_n\cos(n\phi) + b_n\sin(n\phi)], \tag{28}$$

with non-zero coefficients

$$a_0 = Q + h\left(Q^2 + \frac{U^2}{2}\right), \tag{29}$$

$$a_1 = (1 + 2hQ)U, \tag{30}$$

$$b_1 = -\left[Q(3+\Gamma) + h\left(Q^2 + \frac{U^2}{4}\right)(4+\Gamma)\right]T, \tag{31}$$

$$a_2 = \frac{hU^2}{2}, \tag{32}$$

$$b_2 = -[(1+2hQ)(4+\Gamma) - 1]\frac{TU}{2}, \tag{33}$$

$$b_3 = -\frac{4+\Gamma}{4}hTU^2. \tag{34}$$

Similarly to equation (14), we can define Fourier coefficients c_n and corresponding phase lags. Coefficients (29)–(34) are good approximations to the exact Fourier coefficients A_n, B_n of the flux $\bar{F}(\phi_{\rm obs})$ as long as the spot is visible at all phases (through the entire period of

rotation). Alternatively, the pulse profile can be written as a cosine series

$$F(\phi) = Q + h\left(Q^2 + \frac{U^2}{2}\right) + \frac{U(1+2hQ)}{\cos\zeta_1}\cos(\phi+\zeta_1) + \frac{hU^2/2}{\cos 2\zeta_2}\cos[2(\phi+\zeta_2)] + \frac{4+\Gamma}{4}hTU^2\cos\left[3\left(\phi+\frac{\pi}{6}\right)\right], \quad (35)$$

where

$$\tan\zeta_1 = \frac{T}{U}\,\frac{(3+\Gamma)Q + (4+\Gamma)h(Q^2+U^2/4)}{1+2hQ}, \quad (36)$$

$$\tan 2\zeta_2 = \frac{T}{U}\,\frac{(4+\Gamma)(1+2hQ)-1}{h}. \quad (37)$$

The ratio of the harmonic to the fundamental

$$\frac{c_2}{c_1} = \frac{hU}{2(1+2hQ)}\frac{\cos\zeta_1}{\cos 2\zeta_2} \quad (38)$$

grows with the anisotropy parameter h and $\sin i\sin\theta$.

If the spot disappears from the visibility zone for part of the period (classes B, II, and III), the Fourier series becomes infinite. The Fourier coefficients of the light curve can be computed from the coefficients (29)–(34):

$$a'_0 = \frac{\phi_\mathrm{p}}{\pi}\sum_{k=0}^{3} a_k s_k(\phi_\mathrm{p}),$$
$$a'_n = \frac{\phi_\mathrm{p}}{\pi}\sum_{k=0}^{3} a_k\left[s_{n-k}(\phi_\mathrm{p}) + s_{n+k}(\phi_\mathrm{p})\right],$$
$$b'_n = \frac{\phi_\mathrm{p}}{\pi}\sum_{k=1}^{3} b_k\left[s_{n-k}(\phi_\mathrm{p}) - s_{n+k}(\phi_\mathrm{p})\right], \quad (39)$$

where $s_0(\phi) = 1$ and $s_n(\phi) = \sin(n\phi)/(n\phi)$.

Including the time delays further modify the expansions. We are interested in the Fourier coefficients of the function $\bar{F}(\phi_\mathrm{obs}) = F[\phi_\mathrm{obs} - \Delta\phi(\phi)]$. We can calculate the phase delays relative to the photons arriving from the star element closest to the observer (with impact parameter $b = 0$) using equation (19):

$$\Delta\phi(\phi) \approx \Delta\phi(\phi_\mathrm{obs}) \approx \Phi - T\cos\phi_\mathrm{obs}, \quad (40)$$

where $\Phi = \beta_\mathrm{eq}\sqrt{1-u}(1-\cos i\cos\theta) = (1-Q)\beta_\mathrm{eq}/\sqrt{1-u}$. Keeping only the first term in the Taylor expansion, we arrive at

$$\cos n(\phi-\Delta\phi) = \cos n\phi + n\Delta\phi\sin n\phi,$$
$$\sin n(\phi-\Delta\phi) = \sin n\phi - n\Delta\phi\cos n\phi. \quad (41)$$

The Fourier amplitudes for $\bar{F}(\phi_\mathrm{obs})$ are found as follows

$$a''_n = a_n,$$
$$b''_n = b_n + \Phi n a_n - \frac{T}{2}\left[(n-1)a_{n-1} + (n+1)a_{n+1}\right], \quad (42)$$

where we neglected products Tb_n, $\Phi b_n \propto T^2$. If the spot is invisible for a part of the period, one should use coefficients a'_n, b'_n instead of a_n, b_n. For the antipodal spot, we substitute $\theta \to \pi - \theta$ and $\phi \to \pi + \phi$. Thus we still can use the expressions (29)–(34), where Q is replaced by $Q_\mathrm{s} = u - (1-u)\cos i\cos\theta$ and the sign of the odd terms a_1, b_1 and b_3 is changed.

4 RESULTS

We have checked the accuracy of the analytical formalism (Section 3.3) by direct comparison with the exact numerical calculation (Section 2). The accuracy depends mainly on the compactness of the star $u = r_\mathrm{S}/R$ and its rotational frequency ν. Part of the error comes from the light-bending approximation (15); this error increases for stars with large u (Fig. 3). Besides, we made the approximation $\sin\alpha/\sin\psi \approx (1-u)^{1/2}$ in equation (25) for the Doppler factor δ. This introduces an additional error which becomes notable for fast rotators. Errors generally grow at higher ν because we neglected the terms quadratic in β_eq in all formulae.

As an example, we show in Figs 2 and 6 the results for a fast and compact rotator with $\nu = 600$ Hz and $u = 0.4$ ($R/r_\mathrm{S} = 2.5$). In this case, the pulse profile reconstructed from the analytical Fourier amplitudes is very close to the exact profile (Fig. 2). The accuracy of analytical approximation for amplitudes C_0 and C_1 is better than 3 per cent, while C_2 is 15 per cent accurate (see Fig. 6). The phases ζ_1 and ζ_2 (equations 36 and 37, and the phases obtained from equations 39 and 42) are accurate within 0.2 rad. For slower rotation, e.g. $\nu =$ 300 Hz, the error of analytical approximation decreases to $\sim$5 per cent. Only amplitude C_3 (which is smaller than C_1 and C_2 and more sensitive to the neglected terms in the analytical expansion) has a significant error, our formulae underestimate C_3 by about 50 (20) per cent for $\nu = 600$ (300) Hz.

Even for an extremely compact star with $u = 0.5$, the analytical C_1 and C_2 have a good accuracy: they are typically 10–20 per cent smaller than the exact values. Only in the cases with one spot at large colatitudes $\theta > 120^\circ$ and small inclinations $i < 60^\circ$, the amplitudes are underestimated by a factor of 2, because of extreme gravitational bending.

Using the analytical formalism one can understand the behaviour of Fourier amplitudes and their ratio obtained previously by numerical calculations (Weinberg et al. 2001; Muno et al. 2002). Below, we investigate separately the effects of anisotropy and fast rotation.

4.1 Effects of anisotropy

Let us assume a slowly rotating star (i.e. take $\delta = 1$ and $\phi_\mathrm{obs} = \phi$) and investigate the effects of anisotropy $h \neq 0$ of the source emission $I(\alpha) = I_0(1 + h\cos\alpha)$ on the pulse profile. For example, radiation from an optically thin source (slab) is more beamed along the stellar surface and described by $h < 0$ (see e.g. Poutanen & Gierliński 2003; Viironen & Poutanen 2004), while $h \sim 2$ characterizes radiation from an optically thick electron-scattering dominated atmosphere.

As will be seen from equations below, anisotropy (i) introduces harmonic $a_2 \propto h$, (ii) changes the global structure of the profile (e.g. two maxima may appear and $\phi = 0$ may become a minimum) and (iii) leaves the profile symmetric.

We will use the following expression for the flux from a single (or primary) spot,

$$F_\mathrm{p}(\phi) = \cos\alpha_\mathrm{p}(1 + h\cos\alpha_\mathrm{p}), \quad (43)$$

where

$$\cos\alpha_\mathrm{p} = u + (1-u)\cos\psi = Q + U\cos\phi. \quad (44)$$

If secondary (antipodal) spot is present, the corresponding flux is

$$F_\mathrm{s}(\phi) = \cos\alpha_\mathrm{s}(1 + h\cos\alpha_\mathrm{s}), \quad (45)$$

where (using $\cos\psi_\mathrm{s} = -\cos\psi$)

$$\cos\alpha_\mathrm{s} = u - (1-u)\cos\psi = 2u - Q - U\cos\phi. \quad (46)$$

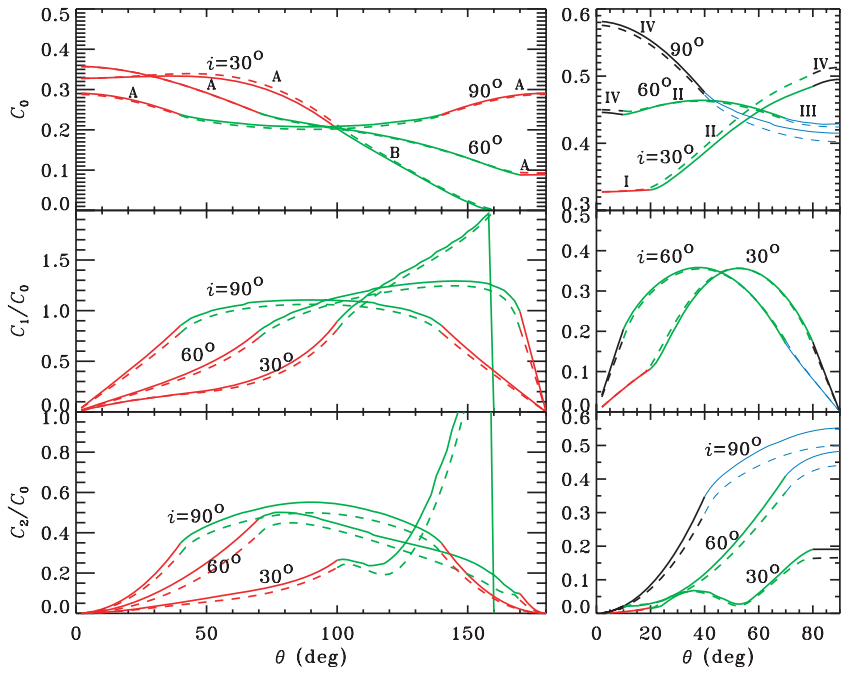

Figure 6. Fourier amplitudes of the pulse profile as functions of the spot colatitude for three inclinations $i = 30^\circ, 60^\circ$ and 90°. Left-hand panel: one spot. Right-hand panel: two antipodal spots. Solid curves show the exact numerical results and dashed curves – the analytical approximation. Inclinations and corresponding visibility classes are marked above the curves. Parameters are $M = 1.4\,\mathrm{M}_\odot, R = 2.5r_\mathrm{S}, \Gamma = 2, \nu = 600$ Hz and $h = -0.7$.

4.1.1 One spot

First, let us consider the simple case of blackbody spots (i.e. $h = 0$). The pulse profile from a single spot then has almost exactly sine shape (B02)

$$F_\mathrm{p}(\phi) = \cos\alpha_\mathrm{p} = Q + U\cos\phi. \tag{47}$$

This immediately gives the non-zero Fourier cofficients $a_0 = Q$ and $a_1 = U$ for pulsars in class A. In class B, the Fourier coefficients can be computed using equations (39). The peak-to-peak amplitude $A \equiv (F_\mathrm{max} - F_\mathrm{min})/(F_\mathrm{max} + F_\mathrm{min})$ is given by

$$A = \begin{cases} \dfrac{U}{Q}, & \text{class A,} \\ 1, & \text{class B.} \\ 0, & \text{class C.} \end{cases} \tag{48}$$

The peak-to-peak amplitude coincides with the ratio $|a_1|/a_0$ and is $\sqrt{2}$ larger than sometimes quoted rms amplitude if the light curve is a pure sine profile.

The pulse profile is given by

$$F(\phi) = Q + h\left(Q^2 + \frac{U^2}{2}\right) + U(1+2hQ)\cos\phi + h\frac{U^2}{2}\cos 2\phi. \tag{49}$$

One sees that anisotropy introduces no phase shift in the harmonics, and the pulse profile remains symmetric about $\phi = 0$ and π; however, the Fourier amplitudes are changed. The amplitude of the fundamental c_1 increases with positive h and decreases if h is negative. The fundamental can even completely disappear when $h = -1/(2Q)$. It is proportional to U and therefore c_1 behaves close to $\sin i \sin\theta$ (see also Fig. 6, left-hand panel for class A and right-hand panel for class I).

Anisotropy $h \neq 0$ introduces harmonic $\cos 2\phi$ in the pulse. The amplitude c_2 of this harmonic can be quite large if h is large (in absolute value) and is proportional to $\sin^2 i \sin^2\theta$ (see equations 32, 33 and lower panels in Fig. 6). The ratio of amplitudes c_2 and c_1 is given by

$$\frac{c_2}{c_1} = \frac{a_2}{a_1} = \frac{hU/2}{1+2hQ} \propto h\sin i\sin\theta. \tag{50}$$

If $h \geqslant -1/2$, the pulse profile has a maximum at $\phi = 0$ and a minimum at $\phi = \pi$. The corresponding pulse amplitude is

$$A = \frac{U(1+2hQ)}{Q + h(Q^2+U^2)}. \tag{51}$$

If $h < -1/2$ and the conditions

$$\cos(i+\theta) < \eta \equiv -\frac{u + 1/2h}{1-u} < \cos(i-\theta) \tag{52}$$

are satisfied, then the pulse has minima at both $\phi = 0$ and π. Two maxima

$$F_\mathrm{max} = -\frac{1}{4h} \tag{53}$$

appear at phases corresponding to

$$\cos\phi = \cos\phi_1 \equiv -\frac{1+2hQ}{2hU}. \tag{54}$$

The global minimum of the pulse profile is at $\phi = \pi$,

$$F_\mathrm{min}(\phi = \pi) = (Q-U)[1 + h(Q-U)]. \tag{55}$$

If $h < -1/2$ and $\cos(i+\theta) > \eta$, the pulse minimum is at $\phi = 0$ and its maximum at $\phi = \pi$. When $\cos(i-\theta) < \eta$, then the minimum is at $\phi = 0$ and the maximum is at $\phi = \pi$.

In class B, the phase $\phi = \pi$ is not visible. The condition for additional maxima (52) is the same as in class A and these maxima are always in the visibility zone, $\cos\phi_1 > \cos\phi_\mathrm{p}$.

The above analysis is also applicable to pulsars with two antipodal spots in class I, when only one spot is visible. Because class I is

smaller on the $\theta - i$ plane than class A, the existence of the maxima at $\phi = |\phi_1|$ (equation [54]) requires a stronger condition on h: $-1/4u < h < -1/2$.

4.1.2 Two antipodal spots

First consider blackbody spots ($h = 0$). In class IV, the pulse profile is flat with $a_0 = 2u$, i.e. there are no pulsations. In class II, the pulse profile consists of a single sinusoidal pulse and a flat plateau appearing when the antipodal spot also becomes visible (see equation 22). In class III, there are two pulses with two plateaus in between (symmetric about phases $\phi = 0$ and π). The primary is seen at $|\phi| < \phi_p$, while the secondary appears at $\cos\phi < \cos\phi_s$. The corresponding pulse amplitudes A for all these classes are given by (B02)

$$A = \begin{cases} \dfrac{U}{Q}, & \text{class I,} \\ \dfrac{U+Q-2u}{U+Q+2u} = \dfrac{\cos(i-\theta)-u}{\cos(i-\theta)+u}, & \text{classes II, III,} \\ 0, & \text{class IV.} \end{cases} \tag{56}$$

The anisotropy $h \neq 0$ modifies significantly the pulse profiles. The analysis is simplest for class IV, where two spots are always visible. Then the total flux is

$$\bar{F}(\phi) = \bar{F}_p(\phi) + \bar{F}_s(\phi) = 2u + h[2(Q-u)^2 + 2u^2 + U^2 + 4(Q-u)U\cos\phi + U^2\cos 2\phi] \tag{57}$$

and the Fourier amplitudes are

$$\frac{c_1}{c_0} = \frac{a_1}{a_0} = \frac{2h(Q-u)U}{u + h[u^2 + (Q-u)^2 + U^2/2]}, \tag{58}$$

$$\frac{c_2}{c_0} = \frac{a_2}{a_0} = \frac{hU^2/2}{u + h[u^2 + (Q-u)^2 + U^2/2]}. \tag{59}$$

The dependencies $c_1/c_0 \propto h \sin 2i \sin 2\theta$ and $c_2/c_0 \propto h \sin^2 i \sin^2\theta$ are found not only in class IV, but also in classes II and III (right-hand panel, Fig. 6). Note that the importance of the second harmonic

$$\frac{c_2}{c_1} = \frac{U}{4(Q-u)} = \frac{1}{4}\tan i \tan\theta \tag{60}$$

is independent of h and grows with i and θ.

If $i + \theta \leqslant 90^\circ$, the pulse profile has two extrema at $\phi = 0$ and π. The pulse peak-to-peak amplitude is

$$A = \frac{2(Q-u)U|h|}{u + h[u^2 + (Q-u)^2 + U^2]}. \tag{61}$$

If $i + \theta > 90^\circ$, there are two additional extrema at $\cos\phi = \cos\phi_2 \equiv -(Q-u)/U = -\cot i \cot\theta$ with

$$F(\phi_2) = 2u(1 + hu). \tag{62}$$

These extrema are minima if $h > 0$ and maxima if $h < 0$. Here $\phi = 0$ is a global maximum for $h > 0$ and a global minimum for $h < 0$. The amplitude of the pulse with four extrema grows with $|h|$,

$$A = \frac{(1-u)^2\ \cos^2(i-\theta)\ |h|}{2u + h[2u^2 + (1-u)^2\ \cos^2(i-\theta)]}. \tag{63}$$

It is maximum at the boundary of class IV when $\cos(i-\theta) = \kappa$.

4.2 Effects of fast rotation

The effects of fast rotation are illustrated in this section with a simple case of blackbody spots ($h = 0$, no anisotropy). Furthermore, we assume that the spots are always visible, i.e. consider classes A, I and IV.

4.2.1 One spot, classes A and I

The flux from one spot is given by

$$F_p(\phi) = \delta^{3+\Gamma}\cos\alpha_p = Q + U\cos\phi - (3+\Gamma)QT\sin\phi - \frac{3+\Gamma}{2}UT\sin 2\phi = Q + \frac{U}{\cos\zeta_1}\cos(\phi+\zeta_1) + \frac{3+\Gamma}{2}UT\cos\left[2\left(\phi+\frac{\pi}{4}\right)\right], \tag{64}$$

which only slightly deviates from a sinusoidal shape. The phase shift

$$\tan\zeta_1 = (3+\Gamma)Q\,\frac{T}{U} \approx \frac{\beta_{eq}}{\sqrt{1-u}}(3+\Gamma)Q \tag{65}$$

is of the order of $\beta_{eq} \ll 1$. The main dependences of the Fourier amplitudes on i and θ are similar to the anisotropic case considered in Section 4.1.1, with c_1 behaving close to $\sin i \sin\theta$ and $c_2 \propto \sin^2 i \sin^2\theta$ (compare equations 30 and 31 as well as equations 32 and 33). The ratio of harmonics is

$$\frac{c_2}{c_1} \approx \frac{(3+\Gamma)T}{2} \approx \frac{(3+\Gamma)}{2}\,\beta_{eq}\sqrt{1-u}\ \sin i\ \sin\theta. \tag{66}$$

We see that the Doppler effect produces the first harmonic and introduces a phase shift between the fundamental and the harmonic, which skews the profile. The phase shift is proportional to β_{eq}.

We note, however, that the ratio c_2/c_1 depends linearly on β_{eq} (which is a small number) and $\sin i \sin\theta$. We conclude that for a single spot $c_2/c_1 \ll 1$, i.e. the Doppler effect alone cannot introduce a strong additional harmonic to the signal (unless Γ is large). In contrast, an anisotropic source can make it easily (see equation 50). In combination with anisotropy, the Doppler effect significantly modifies the pulse profile.

The time delays slightly reduce the phase lag to $\tan\zeta_1 = \beta_{eq}[(4+\Gamma)Q - 1]/\sqrt{1-u}$ and produce a third harmonic with a small amplitude $a_3 \propto UT^2 \propto \beta_{eq}^2$.

4.2.2 Two spots, class IV

The contribution of the secondary (antipodal) spot to the flux is given by

$$F_s(\phi) = \delta_s^{3+\Gamma}\cos\alpha_s = 2u - Q - U\cos\phi + (3+\Gamma)(2u-Q)T\sin\phi - \frac{3+\Gamma}{2}UT\sin 2\phi, \tag{67}$$

where $\delta_s \approx 1 + T\sin\phi$. The total flux is given by

$$F(\phi) = F_p(\phi) + F_s(\phi) = 2u - (3+\Gamma)T[2(Q-u)\sin\phi + U\sin 2\phi]. \tag{68}$$

The time delays introduce the effects of the order β_{eq}^2 which are ignored here.

The Doppler effect modulates the flux, so that the profile is not a plateau anymore. The Fourier amplitudes c_1 and c_2 grow linearly with the rotational frequency and the spectral index Γ. The amplitude of the fundamental,

$$\frac{c_1}{c_0} = \frac{3+\Gamma}{u}(Q-u)\ T \propto \beta_{eq}\sin 2i \sin 2\theta \tag{69}$$

is maximum at the boundary of class IV where $\cos(i-\theta)=\kappa$, while the amplitude of the harmonic,

$$\frac{c_2}{c_0}=\frac{3+\Gamma}{2u}UT \propto \beta_{\rm eq}\sin^2 i\sin^2\theta, \tag{70}$$

is maximum when $i=\theta=90^\circ$. The dependences on i and θ are similar to the anisotropic case from Section 4.1.2. This explains the fact that when both anisotropy and fast rotation are present, the behaviour remains the same (see right-hand panels in Fig. 6). The ratio of the harmonics is

$$\frac{c_2}{c_1}=\frac{U}{2(Q-u)}=\frac{1}{2}\tan i\tan\theta. \tag{71}$$

It differs by a factor of 2 from the anisotropic case (60), and becomes large at large inclination i and spot co-latitude θ.

If $i+\theta\leqslant 90^\circ$, the Doppler-boosted pulse from two antipodal spots has two extrema at

$$\cos\phi=\cos\phi_+\equiv\frac{\sqrt{8+\cot^2 i\cot^2\theta}-\cot i\cot\theta}{4}>0, \tag{72}$$

with maximum at $-\phi_+$ and minimum at ϕ_+. If $i+\theta>90^\circ$, there are two additional extrema at

$$\cos\phi=\cos\phi_-\equiv-\frac{\sqrt{8+\cot^2 i\cot^2\theta}+\cot i\cot\theta}{4}<0, \tag{73}$$

with ϕ_- being the maximum and $-\phi_-$ being the minimum. The global maximum and minimum remain at $\mp\phi_+$.

5 SUMMARY

We have derived an analytical approximation for the pulse profile produced by small spots on a neutron star surface, its Fourier amplitudes and phases. The exact profile is reproduced with good accuracy by our formulae even in the case of very fast rotation (e.g. with the error of ∼15 per cent for rotational frequency $\nu=600$ Hz). For slower rotation of 300 Hz, the accuracy improves to ∼5 per cent. The main advantage of the analytical formalism is that it shows the dependence of the pulse profile and its Fourier series on the parameters of the pulsar.

The proposed formalism can be used to obtain constraints on the neutron star parameters and position of the hotspot from the amplitudes of oscillations observed during X-ray bursts in some low-mass X-ray binaries, as well as from the X-ray pulse profiles of the accretion- and rotation-powered pulsars. Our results can be further extended to study the energy dependence of the profile as well as the effects of the finite spot size.

ACKNOWLEDGMENTS

This research has been supported by the Academy of Finland grant 102181 and the Vilho, Yrjö and Kalle Väisälä Foundation. AMB thanks the Division of Astronomy of the University of Oulu for hospitality during his visit, when this work was finished.

REFERENCES

Beloborodov A. M., 2002, ApJ, 566, L85 (B02)
Gierliński M., Poutanen J., 2005, MNRAS, 359, 1261
Gierliński M., Done C., Barret D., 2002, MNRAS, 331, 141
Leahy D. A., Li L., 1995, MNRAS, 277, 1177
Miller M. C., Lamb F. K., 1998, ApJ, 499, L37
Misner C. W., Thorn K. S., Wheeler J. A., 1973, Gravitation. Freeman, San Francisco
Muno M. P., Özel F., Chakrabarty D., 2002, ApJ, 581, 550
Pechenick K. R., Ftaclas C., Cohen J. M., 1983, ApJ, 274, 846
Poutanen J., 2006, Adv. Space Res., in press (astro-ph/0510038)
Poutanen J., Gierliński M., 2003, MNRAS, 343, 1301
Rybicki G. B., Lightman A. P., 1979, Radiative Processes in Astrophysics. Wiley-Interscience, New York
Strohmayer T., Bildsten L., 2006, in Lewin W. H. G., van der Klis M., eds, Compact Stellar X-Ray Sources. Cambridge Univ. Press, Cambridge, preprint (astro-ph/0301544)
Strohmayer T. E., Markwardt C. B., Swank J. H., in't Zand J., 2003, ApJ, 596, L67
Viironen K., Poutanen J., 2004, A&A, 426, 985
Weinberg N., Miller M. C., Lamb D. Q., 2001, ApJ, 546, 1098
Wijnands R., 2005, Pulsars New Research. Nova Science Publishers, New York, in press (astro-ph/0501264)
Zavlin V. E., Shibanov Yu. A., Pavlov G. G., 1995, Astron. Lett., 21, 149

APPENDIX A: EXACT CALCULATION OF OBSERVED FLUX

A1 Light bending and Lorentz transformations

The exact relation between α and ψ in Schwarzschild geometry (i.e. light bending) is given by (e.g. Misner, Thorn & Wheeler 1973)

$$\psi=\int_R^\infty\frac{{\rm d}r}{r^2}\left[\frac{1}{b^2}-\frac{1}{r^2}\left(1-\frac{r_{\rm S}}{r}\right)\right]^{-1/2}, \tag{A1}$$

where b is impact parameter,

$$b=\frac{R}{\sqrt{1-u}}\sin\alpha, \tag{A2}$$

$u=r_{\rm S}/R$, $r_{\rm S}=2GM/c^2$ is Schwarzschild radius; M and R are mass and radius of the star. The maximum bending angle $\psi_{\rm max}$ corresponds to $\alpha=\pi/2$. The visibility of the spot is defined by a condition $\cos\alpha>0$, or alternatively by $\psi<\psi_{\rm max}\equiv\psi(\alpha=\frac{\pi}{2})$.

As a photon emitted at angle α with respect to the spot normal $\boldsymbol{n}$ propagates to infinity, its direction changes from $\boldsymbol{k}_0$ near the stellar surface to $\boldsymbol{k}$ at infinity, so that $\cos\alpha=\boldsymbol{k}_0\cdot\boldsymbol{n}$ changes to $\cos\psi=\boldsymbol{k}\cdot\boldsymbol{n}$. The relation between $\boldsymbol{k}_0$ and $\boldsymbol{k}$ may be written as

$$\boldsymbol{k}_0=\frac{\sin\alpha\,\boldsymbol{k}+\sin(\psi-\alpha)\,\boldsymbol{n}}{\sin\psi}. \tag{A3}$$

At any moment of time, we can introduce an instantaneous non-rotating frame x,y and z with the y-axis along the direction of the spot motion, x-axis along the meridian towards the equator and z-axis along the normal to the spot. In this static frame,

$$\boldsymbol{k}_0=\left[\frac{\sin\alpha}{\sin\psi}(\sin i\cos\theta\cos\phi-\cos i\sin\theta),\cos\xi,\cos\alpha\right], \tag{A4}$$

where

$$\cos\xi=\frac{\boldsymbol{\beta}}{\beta}\cdot\boldsymbol{k}_0=\frac{\sin\alpha}{\sin\psi}\frac{\boldsymbol{\beta}}{\beta}\cdot\boldsymbol{k}=-\frac{\sin\alpha}{\sin\psi}\sin i\ \sin\phi. \tag{A5}$$

In the frame comoving with the spot (with y-axis along the spot motion, z-axis along the local normal), the unit vector along the photon momentum is obtained from the Lorentz transformation:

$$\boldsymbol{k}_0'=\delta\begin{bmatrix}\dfrac{(\sin i\cos\theta\cos\phi-\cos i\sin\theta)\sin\alpha}{\sin\psi}\\ \gamma(\cos\xi-\beta)\\ \cos\alpha\end{bmatrix}, \tag{A6}$$

where $\gamma=1/\sqrt{1-\beta^2}$ and the Doppler factor

$$\delta=\frac{1}{\gamma(1-\beta\cos\xi)}. \tag{A7}$$

Using equation (A6), we obtain

$$\cos\alpha' = \delta\cos\alpha. \tag{A8}$$

A2 Observed flux

The observed flux from the spot at photon energy E is

$$\mathrm{d}F_E = I_E\,\mathrm{d}\Omega, \tag{A9}$$

where I_E is the specific intensity of radiation at infinity and $\mathrm{d}\Omega$ is the solid angle occupied by spot with area $\mathrm{d}S'$ on the observer's sky. The solid angle can be expressed in terms of the impact parameter

$$\mathrm{d}\Omega = \frac{b\,\mathrm{d}b\,\mathrm{d}\varphi}{D^2}, \tag{A10}$$

where D is the distance to the source and φ is the azimuthal angle corresponding to rotation around line of sight (vector $\boldsymbol{k}$). The impact parameter b depends on ψ only, but not on φ.

Using equation (A2) and the facts that $\mathrm{d}S = R^2\,\mathrm{d}\cos\psi\,\mathrm{d}\varphi$ and $\mathrm{d}S'\cos\alpha' = \mathrm{d}S\cos\alpha$ (since the spot area projected on to the plane perpendicular to the photon propagation direction, i.e. a photon beam cross-section, is Lorentz invariant), one gets

$$\mathrm{d}\Omega = \frac{\mathrm{d}S'\cos\alpha'}{D^2}\,\frac{1}{1-u}\,\frac{\mathrm{d}\cos\alpha}{\mathrm{d}\cos\psi}. \tag{A11}$$

In the limit of weak gravity $u \ll 1$, this gives the usual formula $\mathrm{d}\Omega = \mathrm{d}S'\cos\alpha'/D^2$.

The combined effect of the gravitational redshift and Doppler effect results in the following relation between the monochromatic observed and local intensities (see e.g. Misner et al. 1973; Rybicki & Lightman 1979):

$$I_E = \left(\frac{E}{E'}\right)^3 I'_{E'}(\alpha'), \tag{A12}$$

where $E/E' = \delta\sqrt{1-u}$. Here, $I'_{E'}(\alpha')$ is the intensity computed in the frame comoving with the spot. For the bolometric intensity, one gets

$$I = \left(\delta\sqrt{1-u}\right)^4 I'(\alpha'). \tag{A13}$$

If the radiation spectrum can be represented by a power law $I'_{E'}(\alpha') \propto E'^{-(\Gamma-1)}$ with a photon spectral index Γ which does not depend on the angle α' then

$$I'_{E'}(\alpha') = I'_E(\alpha')\left(\delta\sqrt{1-u}\right)^{\Gamma-1}. \tag{A14}$$

This approximation is equivalent to the assumption of a weak energy dependence of the angular distribution (see Viironen & Poutanen 2004).

The observed spectral flux (equation A9) now reads

$$\mathrm{d}F_E = (1-u)^{1/2}\delta^4 I'_{E'}(\alpha')\cos\alpha\,\frac{\mathrm{d}\cos\alpha}{\mathrm{d}\cos\psi}\,\frac{\mathrm{d}S'}{D^2}, \tag{A15}$$

where we have used the aberration formula (A8). Substituting equation (A14), we recover equation (8).

The bolometric flux is given by

$$\mathrm{d}F = (1-u)\,\delta^5\,I'(\alpha')\cos\alpha\,\frac{\mathrm{d}\cos\alpha}{\mathrm{d}\cos\psi}\,\frac{\mathrm{d}S'}{D^2}. \tag{A16}$$

Thus, the flux from a rapidly rotating star differs by a factor of δ^5 from that from a slowly rotating star (Poutanen & Gierliński 2003). Two powers of δ come from the solid angle transformation, one from the energy, one from the photon arrival time contraction and the fifth from the change in the projected area due to aberration. Aberration may also change the specific intensity since it has to be computed for angle α' in the comoving frame.

A3 Time delays

Finally, we write down here the formula describing the time delays. The delay is caused by different travel times of emitted photons to the observer, depending on the position of the emitting spot. A photon following the trajectory with an impact parameter b is lagging the photon with $b = 0$ by (Pechenick, Ftaclas & Cohen 1983)

$$c\Delta t(b) = \int_R^\infty \frac{\mathrm{d}r}{1-r_\mathrm{S}/r}\left\{\left[1-\frac{b^2}{r^2}\left(1-\frac{r_\mathrm{S}}{r}\right)\right]^{-1/2} - 1\right\}. \tag{A17}$$

For a given pulsar phase ϕ, we compute angle ψ, then we find the corresponding emitted α and the impact parameter using formulae (A1) and (A2), and compute the corresponding delays $\Delta t(b)$ with equation (A17). We then construct a one-to-one correspondence between the pulsar phase ϕ and the photon arrival phase to the observer $\phi_\mathrm{obs} = \phi + \Delta\phi$, with the phase delays

$$\Delta\phi(\phi) = 2\pi\nu\Delta t[b(\phi)]. \tag{A18}$$

For analytical work we can also use the relation $\phi = \phi_\mathrm{obs} - \Delta\phi(\phi) \approx \phi_\mathrm{obs} - \Delta\phi(\phi_\mathrm{obs})$.

This paper has been typeset from a TEX/LATEX file prepared by the author.